Front. Mech. Eng. 2018, 13(3): 411–426
https://doi.org/10.1007/s11465-018-0467-0

RESEARCH ARTICLE

Jianghua FENG, Jing SHANG, Zhixue ZHANG, Huadong LIU, Zihao HUANG

Solid-state transformer-based new traction drive system and control

Abstract A new type of traction drive system consisting of solid-state traction transformer (SSTT), inverter unit, auxiliary inverter, traction motor and other key components is built in order to suit the demand of developing the next-generation electric traction system which will be efficient and lightweight, with high power density. For the purpose of reducing system volume and weight and improving efficiency and grid-side power quality, an efficient SSTT optimized topology combining high-voltage cascaded rectifiers with high-power high-frequency LLC resonant converter is proposed. On this basis, an integrated control strategy built upon synchronous rotating reference frame is presented to achieve unified control over fundamental active, reactive and harmonic components. The carrier-interleaving phase shift modulation strategy is proposed to improve the harmonic performance of cascaded rectifiers. In view of the secondary pulsating existing in a single-phase system, the mathematical model of secondary power transfer is built, and the mechanism of pulsating voltage resulting in beat frequency of LLC resonant converter is revealed, so as to design optimum matching of system parameters. Simulation and experimental results have verified that the traction system and control scheme mentioned in this paper are reasonable and superior and that they meet the future application requirements for rail transit.

Keywords solid-state traction transformer, high-voltage cascaded rectifier, LLC resonant converter, synchronous rotating reference frame, carrier-interleaving phase shift control, secondary pulsating voltage, beat frequency

Received December 26, 2016; accepted May 11, 2017

Jianghua FENG, Jing SHANG, Zhixue ZHANG, Huadong LIU (✉), Zihao HUANG
CRRC Zhuzhou Institute Co., Ltd., Zhuzhou 412001, China
E-mail: liuhd@csrzic.com; hunger5@163.com

1 Introduction

With the construction of electrified railways in China, high-power electric locomotives and high-speed trains are applied, which greatly promotes the economic development. The electric traction technology based on power conversion and alternating current (AC) motor speed adjusting is one of the key technologies of electric locomotive and high-speed electric multiple units. So far, most of them have been applied maturely. The research and development of next-generation electric traction system has begun in China to reach higher speed and greater transport capacity, to effectively reduce energy consumption and to realize energy-saving and emission reduction.

The main objective of next-generation high-speed train traction system is to reduce the volume and weight of the system and to improve efficiency. In the power-decentralized electric multiple units, the traction systems will not be installed intensively anymore; instead, they will be distributed in each compartment of a train. The traction equipment with huge volume will limit the passenger capacity and make structural design of a train more difficult; in addition, the weight of traction equipment will directly affect the acceleration and braking performances of a train, thus affecting the safe operation of the train and passenger comfort. In the traction system, the main traction transformer approximately accounts for 1/3 of the entire equipment [1]. Multiple topologies adopting high frequency transformer (HFT) have been put forward by scholars to reduce the volume and weight of main transformer for train traction and to improve the reliability and flexibility of traction system [2–15]. The idea of such topologies is to have single-phase line-frequency alternating current transformed by power electronic converters into medium-high-frequency alternating current, and then to connect them to high-frequency rectifiers and traction inverters by high-frequency step-down isolation transformers. This new type of converter topology adopting high-voltage multi-level rectifier and high-frequency isolation is known as solid-state transformer [16–19], also called solid-

state traction transformer (SSTT) when it is used in rail transit traction system.

Many studies [20–22] have been carried out addressing various aspects of this type of converters. Among the numerous topologies of SSTT, the most attractive one is the topology combining high-voltage cascaded inverters and DC-DC (DC: Direct current) converters. In this paper, a new type of electric traction system based on SSTT is proposed on the basis of previous researchers. For this topology, H-bridge cascaded rectifiers are used first to convert the high-voltage AC of traction grid into multiple distributed DC busbars; later, LLC isolating type DC-DC converters respectively including an HFT is used to step down the voltage of all DC busbars; and DC voltage is supplied to traction inverter and auxiliary inverter, meanwhile, all DC busbars are isolated from each other. Based on this topology, this paper presents an improved four-quadrant comprehensive control strategy, which is based on synchronous rotating reference frame, and a carrier phase shift control strategy to improve the response speed, control precision, grid-side electric energy quality and anti-interference capability of the system. With respect to inherent secondary pulsation in a single-phase system, this paper derives the mechanism of impact of secondary pulsation on LLC resonant converter, and the impact of secondary pulsation will be suppressed by system optimization.

2 New traction drive system

The main circuit topology of SSTT-based traction drive system is shown in Fig. 1, and it is divided into high-voltage cascaded rectifier, LLC resonant converter, traction inverter and auxiliary inverter. Their functions and features are as follows.

2.1 High-voltage cascaded rectifiers

High-voltage cascaded rectifiers are composed of multiple H-bridge units connected in series, and they are connected into 25 kV high-voltage traction grid with an input inductor L_s. Each H-bridge unit is rectified and then outputs multiple distributed DC voltages at different potentials. The main function of cascaded rectifiers is to maintain the unit power factor at the power grid side, to maintain that the input current is sinusoidal wave, and to keep the distributed DC voltage stable and balanced.

The equivalent switching frequency of AC-side voltage equals to $2N$ (N is the number of H-bridge units connected in series) times the H-bridge unit switching frequency. In general, the switching frequency of an individual H-bridge unit is selected at several hundred Hz to improve the efficiency of a device. Therefore, the number of rectifier output level is large (the maximum number of level is $2N+1$) and the waveform is more like the sinusoidal wave.

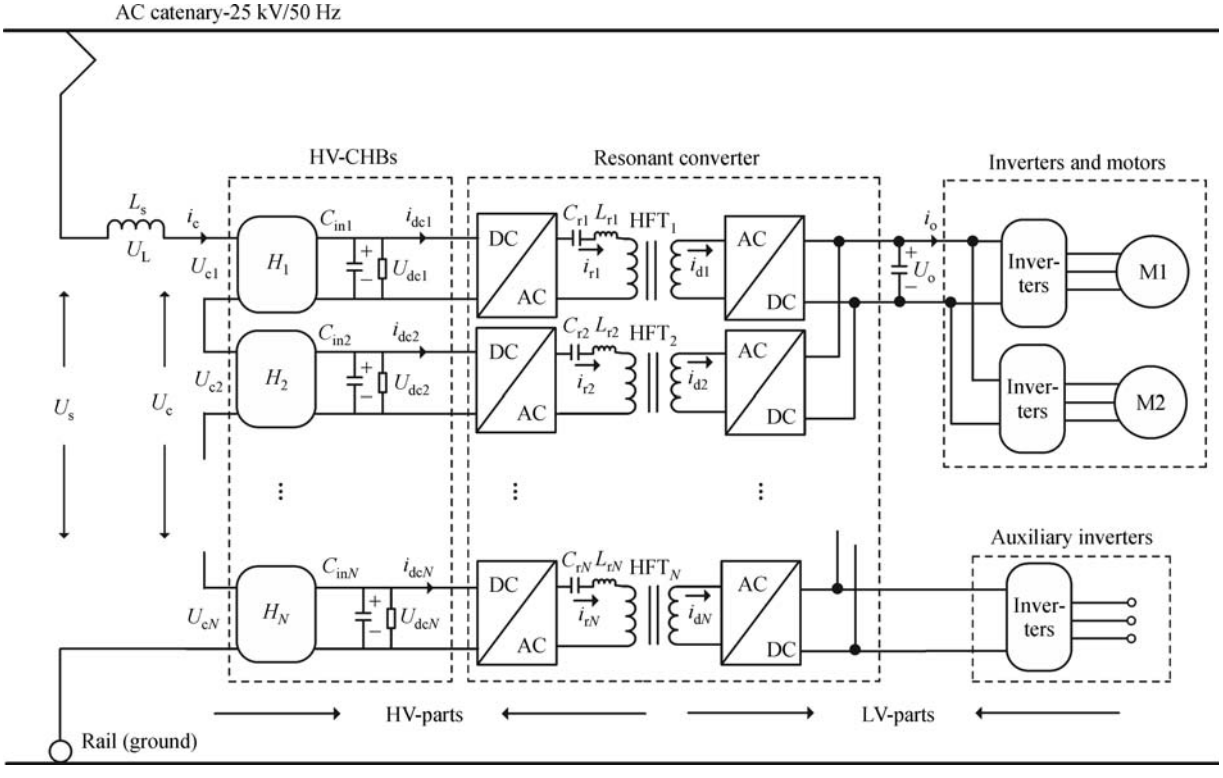

Fig. 1 New traction drive system

Compared to the traditional four-quadrant rectifier, the cascaded rectifiers have incomparable advantages in controlling the grid-side voltage harmonic and current harmonic. Moreover, since the equivalent switching frequency of AC-side voltage waveform is high, the higher harmonic voltage injected in the traction grid is smaller, which is propitious to inhibiting the resonance of train-grid.

In order to improve the reliability and maintainability of the traction system, the H-bridge units of cascaded rectifiers are generally in modular design and have auto-bypass functions. In case of failure of any H-bridge unit, the trouble unit may be automatically isolated, and the device can still operate at full power, and there is no need to reduce the train speed.

2.2 LLC resonant converter

LLC resonant converter converts the multiple DC voltages at different potentials output by the high-voltage cascaded rectifiers into high-frequency square wave, which is coupled to the secondary side through high-frequency isolation transformer later and then is rectified as low-voltage DC output. The voltage conversion is completed, and the high and low potentials are isolated. H-bridges are adopted for both primary-side converters and secondary-side converters, and bidirectional flow of energy can be realized in accordance with traction and braking conditions.

To improve the efficiency of the traction system, resonant elements are used at the primary side of LLC resonant converter to achieve zero voltage switch (ZVS) and small shutdown current within the full load range; and to achieve zero current switch (ZCS) at the secondary side. Generally, to reduce the volume and weight of a device, resonance inductance is integrated in the HFT (including leakage inductance and magnetic inductance), but this will pose higher requirements for the technological level of HFT.

2.3 Traction inverter and motor

The traction inverter controls the motor to output corresponding torque in accordance with system command to achieve traction, braking and inert operations and to meet the demand of the system for precise control over the traction torque. The maximum switching frequency of traction inverter is limited by heat radiation system and the maximum switching frequency of traction inverter of general high-speed electric multiple units and heavy-load locomotive is only several hundred Hz [23], since the electric locomotive traction drive system is characterized by very high voltage, large current, high power; at the same time, because the locomotive operates in the wide speed scope, the variation range of modulation ratio of traction inverter is very large. In case of operation at low switching frequency, the reduction of modulation ratio makes the harmonic content in the output voltage and current of traction inverter increase greatly, which results in increase of motor loss, severe heat and larger noise [24]. In the SSTT-based new traction drive system, since SSTT has wide DC voltage output range, the output DC voltage of SSTT, namely input voltage of traction inverter, can be reduced by corresponding control strategy when the output voltage of traction inverter is lower, so as to effectively improve the modulation ratio of traction inverter and to reduce output harmonic content and noise.

2.4 Auxiliary inverter

The main function of auxiliary inverter is to convert the DC voltage into standard three-phase voltage output to feed the traction motor fan, traction inverter water pump, air-conditioner compressor and other three-phase AC loads. Auxiliary inverter is connected to the public DC busbar of SSTT, which is more conducive to the power balance of the whole traction system, by comparison to the traditional traction system in which separate auxiliary inverter windings need to be provided.

The control targets of SSTT cascaded rectifiers are the waveform and phase angle of grid-side current and the size of intermediate DC voltage, and there is no essential difference between it and the four-quadrant rectifier of existing electric traction system. Therefore, theoretically, all control methods applicable to traditional four-quadrant rectifier apply to SSTT cascaded rectifiers. However, since the SSTT is a single-phase high-voltage high-power cascaded rectifier that is vertically hanging from the traction grid and is connected to LLC consonant converter, the load, a lot of work concerning control strategy in increasing the system response speed and control precision of SSTT, and in controlling the degree of unbalance of cascaded rectifier voltage, has to be done.

Due to the single-phase characteristics of SSTT cascaded rectifier, there must be secondary voltage pulsation in DC voltage. As shown in Fig. 1, after the DC voltage of cascaded rectifier has been modulated by LLC resonant converter, there will be beat frequency controlled by similar motors in the resonant current [25], which will greatly reduce the scope of soft switch and affect the safe operation of the inverter. Meanwhile, there is also secondary voltage pulsation in the DC voltage from LLC resonant converter, which will bring about great trouble in control of traction inverter. Thus, it is necessary to control the impact of secondary pulsating voltage on traction inverter in terms of both system design and control strategy.

3 High-voltage cascaded rectifier control strategy

3.1 Control of fundamental wave of SSTT cascaded rectifier

The idea of fundamental current control of SSTT cascaded

rectifier based on synchronous rotating reference frame [26]: Through conversion of synchronous rotating reference frame, the physical quantity of single-phase rectifier is reflected on the d-q axes, and then the direct current physical quantities of d-q axes are controlled respectively. Through transformation of synchronous rotating reference frame, the AC current signal is transformed into DC signal and is controlled by Proportional Integral (PI) regulator, so as to control the active component and reactive component of current without steady-state error. The control principle of fundamental current is as shown in Fig. 2.

3.1.1 Outer voltage loop design based on instantaneous power balance

The equivalent circuit diagram of SSTT cascaded rectifier is shown in Fig. 3. The output voltages of cascaded H-bridges as indicated in Fig. 1 are respectively U_{c1}, U_{c2},...,U_{cN}, and N is the number of cascaded power unit. Connect all power supplies in series to output the phase voltage U_c. The electric potential difference between U_c and grid voltage U_s will be superposed on the connection reactance L_s, thus producing current i_c. DC-DC converter, traction inverter and motor (M1, M2) can be equivalent to a time-varying resistor R_L, the capacitor current is i_{cap}, the equivalent voltage at the DC side is U_{dc} and the equivalent DC current is i_{dc}.

As shown in Fig. 3, the instantaneous active power at the grid side is equal to the active power at the DC side in case of no regard for the loss of connection inductance and H-bridge module.

$$P_{net} = P_{dc}. \tag{1}$$

Under d-q reference system, the active power at the grid side can be expressed as

$$P_{net} = U_{sd} i_{cd} + U_{sq} i_{cq}, \tag{2}$$

where, i_{cd} and i_{cq} are the d-q components of i_c current , and U_{sq} is 0 at the time of selecting axis d of synchronous reference frame to be synchronous with grid voltage U_s, and thus

$$P_{net} = U_{sd} i_{cd}. \tag{3}$$

Power at the DC side is

$$P_{dc} = P_L + P_{cap} = U_{dc}\frac{U_{dc}}{R_L} + U_{dc} i_{dc}. \tag{4}$$

Since $i_{dc} = C\frac{dU_{dc}}{dt}$, Eq. (4) can be expressed as

$$P_{dc} = \frac{U_{dc}^2}{R_L} + \frac{1}{2}C\frac{dU_{dc}^2}{dt}. \tag{5}$$

Calculate according to Eqs. (1), (3) and (5),

$$i_{cd} = \left(\frac{U_{dc}^2}{R_L} + \frac{1}{2}C\frac{dU_{dc}^2}{dt}\right)\Big/ U_{sd}. \tag{6}$$

Then, the PI controller is introduced to calculate,

$$i_{cd} = \left\{\frac{U_{dc}^2}{R_L} + \left[K_p(U_{dcref}^2 - U_{dc}^2) + K_i\int(U_{dcref}^2 - U_{dc}^2)dt\right]\right\} / U_{sd}. \tag{7}$$

As a result, the design idea of outer voltage loop based

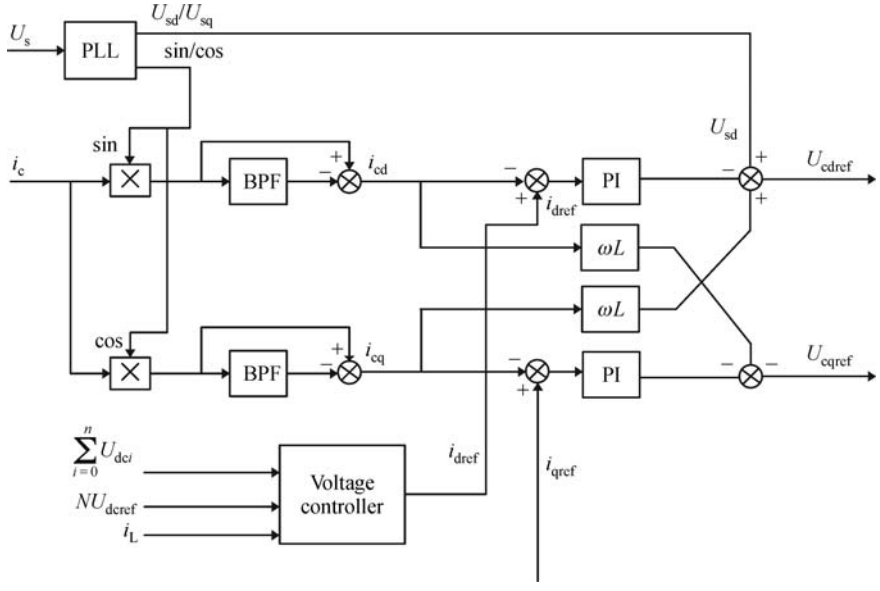

Fig. 2 Fundamental current control principle based on synchronous rotating reference frame. BPF: Band pass filter; PLL: Phase-locked loop

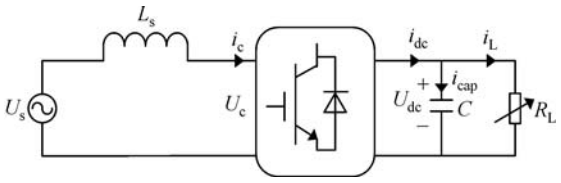

Fig. 3 Equivalent circuit diagram of SSTT cascaded rectifier

on instantaneous power balance is that collect the DC-side voltages of all H-bridge units of cascaded topology; calculate the sum of such voltages and square the sum; obtain the difference between the sum squared and the square of sum of DC voltage reference values; carry out PI adjustment and obtain the power of capacitance. Plus the load power to obtain the total power at the DC side, and then transform the total power at the DC side into the reference quantity of current i_{dref}. Meanwhile, to prevent second harmonic from being introduced into the controller, fast moving average filter (FMAF) and root-mean-square (RMS) of DC voltage and load current are calculated to filter and remove second and other even harmonics. Since the design idea of outer voltage loop is to directly adjust the power of rectifier and to introduce the voltage component of grid for calculation, the outer voltage loop (as shown in Fig. 4) based on instantaneous power balance has strong immunity to interference when the load changes and the grid voltage fluctuates; moreover, the outer voltage loop is of very fast response speed.

3.1.2 Inner loop current control

The equivalent circuit diagrams of cascaded rectifier on d and q planes are shown in Fig. 5.

According to Fig. 5, grid-side mathematical model of cascaded rectifier is a multivariable coupling and linearized model.

$$\begin{cases} \dfrac{\mathrm{d}i_{cd}}{\mathrm{d}t} = \dfrac{1}{L}U_{sd} + \omega i_{cq} - \dfrac{1}{L}U_{cd} \\ \dfrac{\mathrm{d}i_{cq}}{\mathrm{d}t} = \dfrac{1}{L}U_{sq} - \omega i_{cd} - \dfrac{1}{L}U_{cq} \end{cases}. \tag{8}$$

It is expressed in the form of state equation:

$$\begin{bmatrix} \dfrac{\mathrm{d}i_{cd}}{\mathrm{d}t} \\ \dfrac{\mathrm{d}i_{cq}}{\mathrm{d}t} \end{bmatrix} = \begin{bmatrix} 0 & \omega \\ -\omega & 0 \end{bmatrix} \begin{bmatrix} i_{cd} \\ i_{cq} \end{bmatrix} + \frac{1}{L} \begin{bmatrix} U_{sd} - U_{cd} \\ U_{sq} - U_{cq} \end{bmatrix}, \tag{9}$$

where i_{cd} and i_{cq} are state variables, U_{sd} and U_{sq} are d-q variables of grid voltage U_s, U_{cd} and U_{cq} are d-q variables of cascaded rectifier output voltage U_c.

According to the equations above, there is a coupling between variable of axis d and that of axis q in mathematical model. Adoption of feedforward decoupling strategy is considered to introduce voltage coupling compensation items $\omega L i_{cd}$ and $\omega L i_{cq}$, as well as traction grid voltage feed forward items U_{sd} and U_{sq}. When PI decoupling control is used, the voltage commands U_{cdref} and U_{cqref} controlled by fundamental wave are

$$\begin{cases} U_{cdref} = U_{sd} + \omega L i_{cq} - \left[k_{p1}(i_{dref} - i_{cd}) + k_{i1}\int (i_{dref} - i_{cd})\mathrm{d}t \right] \\ U_{cqref} = U_{sq} + \omega L i_{cd} - \left[k_{p2}(i_{qref} - i_{cq}) + k_{i2}\int (i_{qref} - i_{cq})\mathrm{d}t \right] \end{cases}. \tag{10}$$

3.2 Low-order harmonic self-suppression technology

As the goal of SSTT is to reduce volume and weight, the cascaded rectifier adopts high-voltage high-power module. The support capacitance is small while the dead time of high-voltage high-power module is long; moreover, the second-harmonic generation fluctuation at the DC side will become greater, and a large number of low-order harmonics, including the 3rd-, the 5th- and the 7th-order harmonics, will be generated in the cascaded rectifier current i_c. Therefore, it is also necessary to design harmonic suppression algorithm for SSTT cascaded rectifier control strategy, so as to suppress the low-order harmonics generated by cascaded rectifier. For suppression of specific-order harmonics, rapid and accurate analysis of designated-order harmonics is a prerequisite for control. Proceeding from the accuracy and real-time performance of digital control, a harmonic detection method which is based on digital band pass and multiple synchronous rotating reference systems is presented.

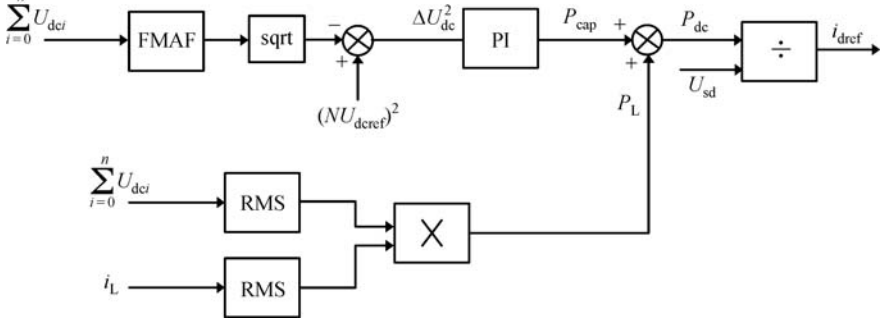

Fig. 4 Voltage loop based on instantaneous power balance

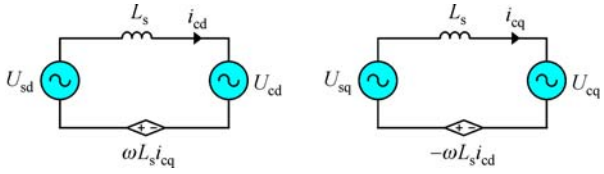

Fig. 5 Equivalent circuit diagrams of cascaded rectifier on d and q planes

The detection principle of specific-order harmonics is indicated in Fig. 6. The cut-off frequency of band pass filter (BPF) is set as the frequency of n-order harmonic ($n \geqslant 1$), for instance, for the fifth-order harmonic, the frequency of BPF is set as 250 Hz; extract the n-order harmonic component from current i_c to obtain n-order harmonic component i_{cn} of current; the sine and cosine ($\sin\omega t$,$\cos\omega t$) of fundamental wave phase position information are obtained through phase locking loop of grid voltage U_s. After that, frequency multiplication algorithm is adopted to obtain values of the phase position information of grid voltage n-order harmonics; make n-order harmonic component i_{cn} be subject to synchronous rotating d-q transformation as mentioned in section 3.1, so as to calculate the instantaneous values i_{cdn} of active and reactive components of i_{cn} in d-q reference frame; decoupling control of current by i_{cqn} is achieved by using the resistance value $n\omega L$ of connection reactance under n-order harmonic, thus obtaining the voltage commands U_{cdn} and U_{cqn} under d-q synchronous reference system; again, conduct d-q reverse transformation to get the voltage command U_{ref}^{n} of n-order harmonic, which will be equally distributed to all cascaded modules to calculate U_{iref}^{n}.

In Fig. 6, when $n = 1$, namely the current is fundamental wave, the active current reference value i_{dref} is the active component of fundamental current adjusted by DC-side voltage controller, and the DC-side voltage is regulated by controlling the active component of fundamental wave flowing into the inverter current. i_{qref} is zero in case of full compensation for reactive current of the grid, so as to ensure the reactive power of grid is zero. When $n \geqslant 1$, both active current reference value i_{dref} and reactive current reference value i_{qref} are zero to completely offset n-order current harmonics.

Upon getting the voltage command U_{iref}^{n} (n is the harmonic order, $n = 3,5,7,11,...$) of each H-bridge unit that suppresses each order harmonic current as shown in Fig. 7, all voltage commands shall be superposed to gain the total reference voltage command U_{i_all} of a certain module of cascaded rectifier. Finally, compare the total reference voltage with triangular wave and conduct sinusoidal pulse width modulation (SPWM) to obtain the trigger pulse of a certain module of cascaded rectifier.

3.3 Carrier-interleaving phase shift PWM technology

According to Refs. [27,28], carrier phase shift sinusoidal pulse width modulation (CPS-SPWM) is generally used for H-bridge cascaded rectifier. The Fourier expression of output voltage of a single H-bridge unit is as follows:

$$U_h = U_{dc}\left\{m\sin\omega t + \sum_{n=1}^{\infty}\left[\frac{4}{n\pi}\cos\frac{n\pi}{2}\sin\left(\frac{mn\pi}{2}\sin\omega t\right)\cos n\theta\cos n\omega_c t\right] + \sum_{n=1}^{\infty}\left[\frac{4}{n\pi}\cos\frac{n\pi}{2}\sin\left(\frac{mn\pi}{2}\sin\omega t\right)\sin n\theta\sin n\omega_c t\right]\right\}, \tag{11}$$

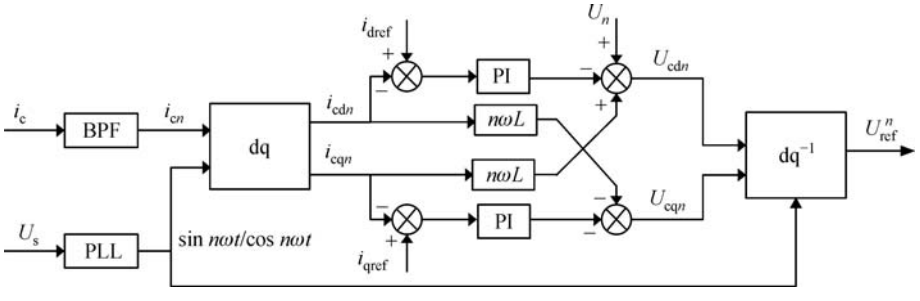

Fig. 6 Certain-order harmonic current detection and control

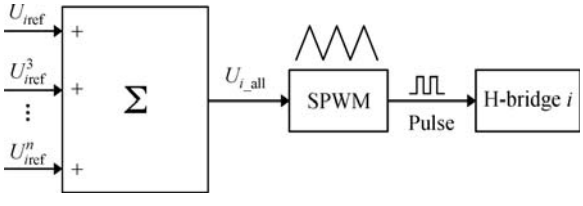

Fig. 7 Current harmonics control principle

where U_h is the voltage of a single H-bridge unit, U_{dc} is the voltage at the DC side, m is the modulation depth, ω is the angular frequency of grid voltage, and ω_c is the angular frequency of carrier wave.

As indicated in Fig. 1, assume the DC voltages of N number of H-bridge units are equal, expressed as U_{dc}, thus the Fourier expression of voltage U_{ig} of the ith module to ground after cascading is

$$\begin{aligned}U_{ig} = U_{dc}\Bigg\{ & m\sin\omega t + \sum_{n=1}^{\infty}\left[\frac{4}{n\pi}\cos\frac{n\pi}{2}\sin\left(\frac{mn\pi}{2}\sin\omega t\right)\cos n\theta_i\cos n\omega_c t\right] + \sum_{n=1}^{\infty}\left[\frac{4}{n\pi}\cos\frac{n\pi}{2}\sin\left(\frac{mn\pi}{2}\sin\omega t\right)\sin n\theta_i\sin n\omega_c t\right] \\ & + m\sin\omega t + \sum_{n=1}^{\infty}\left[\frac{4}{n\pi}\cos\frac{n\pi}{2}\sin\left(\frac{mn\pi}{2}\sin\omega t\right)\cos n\theta_{i+1}\cos n\omega_c t\right] \\ & + \sum_{n=1}^{\infty}\left[\frac{4}{n\pi}\cos\frac{n\pi}{2}\sin\left(\frac{mn\pi}{2}\sin\omega t\right)\sin n\theta_{i+1}\sin n\omega_c t\right] + ... + m\sin\omega t \\ & + \sum_{n=1}^{\infty}\left[\frac{4}{n\pi}\cos\frac{n\pi}{2}\sin\left(\frac{mn\pi}{2}\sin\omega t\right)\cos n\theta_N\cos n\omega_c t\right] + \sum_{n=1}^{\infty}\left[\frac{4}{n\pi}\cos\frac{n\pi}{2}\sin\left(\frac{mn\pi}{2}\sin\omega t\right)\sin n\theta_N\sin n\omega_c t\right]\Bigg\}.\end{aligned} \tag{12}$$

Calculate according to Eq. (12):

$$\begin{aligned}U_{ig} = {} & (N-i)U_{dc}m\sin\omega t + U_{dc}\sum_{n=1}^{\infty}\left[\frac{4}{n\pi}\cos\frac{n\pi}{2}\sin\left(\frac{mn\pi}{2}\sin\omega t\right)\cos n\omega_c t(\cos n\theta_i + \cos n\theta_{i+1} + ... + \cos n\theta_N)\right] \\ & + U_{dc}\sum_{n=1}^{\infty}\left[\frac{4}{n\pi}\cos\frac{n\pi}{2}\sin\left(\frac{mn\pi}{2}\sin\omega t\right)\sin n\omega_c t(\sin n\theta_i + \sin n\theta_{i+1} + ... + \sin n\theta_N)\right],\end{aligned} \tag{13}$$

$$\begin{cases} X = \sin n\theta_i + \sin n\theta_{i+1} + ... + \sin n\theta_N \\ Y = \cos n\theta_i + \cos n\theta_{i+1} + ... + \cos n\theta_N \end{cases}. \tag{14}$$

In the Equation above, θ_i is the carrier phase shift angle of the ith $(1 \leqslant i \leqslant N)$ module. When CSP-SPWM technology is adopted, the carrier wave of each H-bridge unit will increase successively, namely,

$$\begin{cases} X = \sin\frac{n(i-1)\pi}{N} + \sin\frac{ni\pi}{N} + ... + \sin\frac{(N-1)\pi}{N} \\ Y = \cos\frac{n(i-1)\pi}{N} + \cos\frac{ni\pi}{N} + ... + \cos\frac{(N-1)\pi}{N} \end{cases}. \tag{15}$$

In Eq. (12), in case n is an odd number, $\cos\frac{n\pi}{2} = 0$; so, calculation is only required when n is an even number. If $i = 1$, U_{ig} will be the total output voltage of cascaded rectifier, namely,

$$\begin{cases} X = \sin\frac{0\pi}{N} + \sin\frac{\pi}{N} + ... + \sin\frac{(N-1)\pi}{N} \\ Y = \cos\frac{0\pi}{N} + \cos\frac{\pi}{N} + ... + \cos\frac{(N-1)\pi}{N} \end{cases}. \tag{16}$$

Combining Eqs. (12) and (16), we can see that the total output voltage remains unchanged and the grid current characteristics will not change in case of arbitrary exchange of phase shift angles of H-bridge units of cascaded rectifier. However, upon exchange of phase shift angles of H-bridge units, the results of Eq. (15) of the ith $(i \neq 1)$ H-bridge unit will vary, namely the voltage U_{ig} of the ith H-bridge unit to ground will change. If exchange of phase shift angles can help to reduce the voltage of the ith module to ground and the change rate of voltage, the insulation grade of module can be reduced. For instance, if the phase shift angles of two adjacent modules are respectively $\frac{j-1}{N}\pi$ and $\frac{N-j}{N}\pi$ $(1 \leqslant j \leqslant N)$, it will not be difficult to prove that X in Eq. (15) approximates to 0 in case i is an even number, which means that the harmonic of voltage to ground of the ith module will decrease.

4 Effect mechanism of secondary voltage on LLC resonant converter and optimized design

4.1 LLC beat frequency

As shown in Fig. 1, secondary voltage occurs in the DC voltage outputted by the cascaded rectifier due to characteristics of the single-phase system [29]. In the following paragraphs, the impact of secondary voltage on operating scope of the soft switch of the LLC resonant

converter will be deduced. On the basis of optimized design of system and control strategy, further discussion will be conducted on mitigating the impact of secondary voltage on the LLC resonant converter so as to improve system safety and reliability.

As shown in Fig. 8, U_{dc} represents the output DC voltage on a certain H-bridge of the cascaded rectifier; L_r and L_m separately stand for leakage inductance and magnetic inductance of the high-frequency transformer HFT; C_r represents the resonant capacitance, while U_o represents the output DC voltage.

Assume the input voltage U_{dc} to be

$$U_{dc} = U_{dc0} + U_2 \sin\omega_2 t, \tag{17}$$

where U_{dc0} is DC component, U_2 is magnitude of secondary voltage, and ω_2 is angular frequency of secondary voltage.

The input voltage U_{dc} sequentially passes Q1, Q2, Q3 and Q4 before being inverted into the square-wave voltage in the duty ratio of 50%, with the switch frequency being f_s. It is equivalent to a positive-negative square-wave signal with the frequency of f_s and magnitude of 1, on the basis of which U_{dc} is sampled and U_{ab} is thus obtained. Magnitude of secondary voltage. Angular frequency of secondary voltage, namely,

$$U_{ab} = S(\omega_s t) U_{dc}, \tag{18}$$

where

$$S(\omega_s t) = \begin{cases} 1 & \omega_s t \rightarrow (0,\pi] \\ -1 & \omega_s t \rightarrow (-\pi,0) \end{cases}. \tag{19}$$

Conduct Fourier decomposition on the periodic functional Eq. (19),

$$S(\omega_s t) = \sum_{n=1}^{N} \left(\frac{4}{n\pi} \sin n\omega_s t \right), \; n = 1,3,5,... \tag{20}$$

Substitute Eqs. (17) and (19) into Eq. (18),

$$U_{ab} = \sum_{n=1}^{N} \left[\frac{4}{n\pi} (U_{dc0} + U_2 \sin\omega_2 t) \sin n\omega_s t \right], \; n = 1,3,5,... \tag{21}$$

As the voltage magnitude is almost negligible when $n \geqslant 3$, and the resistance of the LC resonant loop becomes very high in the frequency band of $n \geqslant 3$, it is unnecessary to take account of the current generated by voltage when $n \geqslant 3$ and only the condition when $n = 1$ is considered. Then,

$$U_{ab} = \frac{4}{\pi} (U_{dc0} + U_2 \sin\omega_2 t) \sin\omega_s t. \tag{22}$$

Conduct trigonometric operation on Eq. (22),

$$U_{ab} = \frac{4}{\pi} U_{dc0} \sin\omega_s t - \frac{2}{\pi} U_2 \cos(\omega_s + \omega_2) t + \frac{2}{\pi} U_2 \cos(\omega_s - \omega_2) t. \tag{23}$$

According to Eq. (23), the input voltage excitation U_{ab} of the resonant circuit not only contains the ω_s component, but the $(\omega_s + \omega_2)$ and $(\omega_s - \omega_2)$ components (also called the difference frequency component) as well. Usually, $\omega_s \gg \omega_2$. Resistances of three frequency components are quite close, approximating to zero in case of LC resonance. In this case, a small difference frequency voltage produces a large current, similar to the beat frequency phenomenon in motor control. The superposition of these two component currents result in abnormal fluctuation of the resonant current and affects the operating scope of ZVS of the LLC resonant converter. Quantitative deduction on the difference frequency components of resonant currents i_r and i_d will be conducted as follows.

4.2 Quantitative deduction on difference frequency component

Assume that the circuit gain of the LLC resonant converter is K and the turn ratio of the high-frequency transformer is M. When sub-characteristic harmonic voltage of the switch is ignored, the output voltage U_o can be expressed as follows,

$$U_o = \frac{K}{M} (U_{dc0} + U_2 \sin\omega_2 t). \tag{24}$$

Then, current of the output capacitance C_o will be

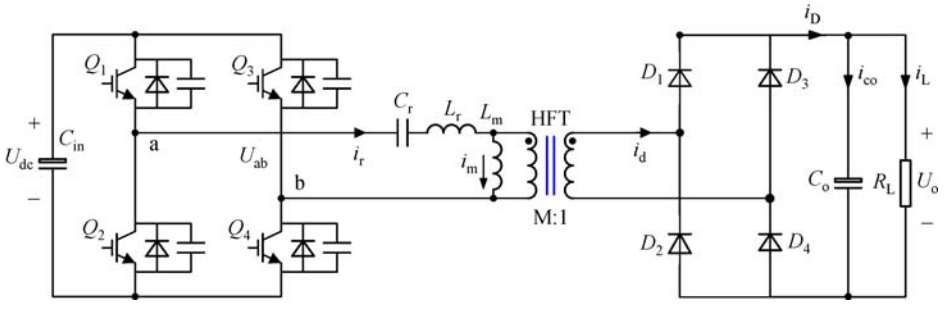

Fig. 8 Schematics of the LLC resonant converter

$$i_{C_o} = C_o \frac{\mathrm{d}U_o}{\mathrm{d}t} = \frac{K}{M} C_o \frac{\mathrm{d}(U_{dc0} + U_2 \sin\omega_2 t)}{\mathrm{d}t}. \quad (25)$$

Calculate according to Eq. (25),

$$i_{C_o} = \frac{K}{M} \omega_2 C_o U_2 \cos\omega_2 t. \quad (26)$$

Equation for the load current:

$$i_L = \frac{U_o}{R_L} = \frac{K}{M}\left(\frac{U_{dc0}}{R_L} + \frac{U_2 \sin\omega_2 t}{R_L}\right). \quad (27)$$

As

$$i_D = i_{C_o} + i_L. \quad (28)$$

Substitute Eqs. (26) and (27) into Eq. (28):

$$i_D = \frac{K}{M} \omega_2 C_o U_2 \cos\omega_2 t + \frac{K}{M}\left(\frac{U_{dc0}}{R_L} + \frac{U_2 \sin\omega_2 t}{R_L}\right). \quad (29)$$

As the time sequence for rectifier conduction and switch of the diode on the secondary side of the LLC resonant converter is completely consistent with that of insulated gate bipolar transistor (IGBT) of the primary side, after rectification of i_d by the diode, it is also equivalent to a positive-negative square-wave signal with the frequency of f_s and magnitude of 1, on the basis of which i_D is sampled and thus i_2 is obtained.

Same as Eq. (18):

$$i_d = S(\omega_s t) i_D, \quad (30)$$

where $S(\omega_s t)$ is expressed as Eq. (19).

Substitute Eq. (19) into Eq. (30) to get

$$i_d = \sum_{n=1}^{N} \frac{4}{n\pi} i_D \sin n\omega_s t,\ n = 1,3,5,... \quad (31)$$

If only $n = 1$ is taken account of, then

$$i_d = \frac{4}{\pi}\frac{K}{M}\sin\omega_s t\left[C_o U_2 \omega_2 \cos\omega_s t + \left(\frac{U_{dc0}}{R_L} + \frac{U_2 \sin\omega_2 t}{R_L}\right)\right]. \quad (32)$$

Obtain

$$i_d = \frac{4}{\pi}\frac{K}{M}\frac{U_{dc0}}{R_L}\sin\omega_s t + \frac{4}{\pi}\frac{K}{M}\omega_2 C_o U_2 \sin\omega_s t \cos\omega_2 t + \frac{4}{\pi}\frac{K}{M}\frac{U_2}{R_L}\sin\omega_s t \sin\omega_2 t. \quad (33)$$

According to results of trigonometric operation, i_d mainly contains three frequency components: ω_s and $(\omega_s - \omega_2)$, $(\omega_s + \omega_2)$, which are separately expressed as follows:

$$i_d(\omega_s) = \frac{4}{\pi}\frac{K}{M}\frac{U_{dc0}}{R_L}\sin\omega_s t, \quad (34)$$

$$i_d(\omega_s - \omega_2) = \frac{2}{\pi}\frac{K}{M}\left[\omega_2 C_o U_2 \sin(\omega_s - \omega_2)t + \frac{U_2}{R_L}\cos(\omega_s - \omega_2)t\right], \quad (35)$$

$$i_d(\omega_s + \omega_2) = \frac{2}{\pi}\frac{K}{M}\left[\omega_2 C_o U_2 \sin(\omega_s + \omega_2)t + \frac{U_2}{R_L}\cos(\omega_s + \omega_2)t\right]. \quad (36)$$

According to Fig. 8,

$$i_r = \frac{i_D}{M} + i_m, \quad (37)$$

where

$$i_m = \frac{U_{ab}}{j\omega L_m} = \sum_{n=1}^{N}\left(\frac{4}{n\pi}\frac{(U_{dc0} + U_2 \sin\omega_2 t)\sin n\omega_s t}{j\omega_n L_m}\right),\ n = 1,3,5,... \quad (38)$$

According to Eq. (38), excitation current i_m also contains the difference frequency current. As calculation results show, the difference frequency components of $(\omega_s - \omega_2)$ in i_m is far less than that in i_d, As a result, the difference frequency components in the resonant current of the primary side i_r are mainly determined by Eqs. (35) and (36).

4.3 Optimized design for beat frequency suppression

According to Eqs. (34) and (35), if $U_2 = 0$, that is, the secondary voltage in $U_{dc} = 0$ is zero, there will be no difference frequency component in the resonant current. Reference [30] summarizes three methods to suppress secondary voltage component. Whichever method is adopted, it is necessary to use an additional auxiliary circuit. Such method of increasing volume and weight is in fact against the design concept for the next generation of traction system that is based on SSTT, thus will not be adopted.

Assume vectors A and B to be:

$$A = \frac{2}{\pi}\frac{K}{M}\omega_2 C_o U_2 \sin(\omega_s - \omega_2)t, \quad (39)$$

$$B = \frac{2}{\pi}\frac{K}{M}\frac{U_2}{R_L}\cos(\omega_s - \omega_2)t. \quad (40)$$

Assume that vectors C and D are separately the difference frequency components of $(\omega_s - \omega_2)$ and $(\omega_s + \omega_2)$. Substitute Eqs. (39) and (40) into Eqs. (35) and (36) to obtain

$$C = A + B, \tag{41}$$

$$D = A - B. \tag{42}$$

As shown in Fig. 9, under the same power condition, vector B remains unchanged, thus it is practical to reduce the difference frequency component by reducing vector A, which, theoretically, can be reduced to the same value as vector B. According to Eq. (39), when the switch frequency remains unchanged, vector A can be reduced by reducing the output capacitance C_o, and thus to reduce the difference frequency component. Therefore, in actual design, it is a good practice to minimize capacitance C_o and properly increase the input capacitance C_{in} to reduce the difference frequency component on the basis of fully taking account of the scope of the soft switch of the LLC resonant converter, the allowable scope of fluctuation of secondary voltage and volume of equipment.

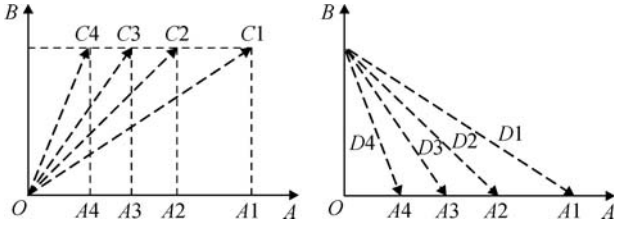

Fig. 9 Vector diagram of difference frequency components

5 Simulation and experimental verification

5.1 Simulation verification of the carrier-interleaving phase shift control strategy

A high-voltage cascaded rectifier simulation model is established to verify the carrier-interleaving phase shift control strategy mentioned in Section 3.3, as shown in Table 1.

Table 1 Parameters of the simulation model

Parameters	Value
Grid voltage, U_s/kV	25
Rated power/(kV·A)	1800
Cells of cascaded	13
HV-CHB cell switch frequency/Hz	450
Carrier phase-shift angle	π/13

The carrier phase shift control strategy is adopted for the cascaded rectifier and phase shift is conducted sequentially: 0, $\frac{\pi}{13}$, ..., $\frac{12\pi}{13}$. Then, voltages to earth of the 7th and 8th H-bridge units of the cascaded rectifier are tested.

The carrier interleaving phase shift control strategy is adopted for the cascaded rectifier and phase shift is conducted sequentially: 0, $\frac{12\pi}{13}$, $\frac{\pi}{13}$, $\frac{11\pi}{13}$, ..., $\frac{5\pi}{13}$, $\frac{7\pi}{13}$. Then, voltages to earth of the 7th and 8th H-bridge units of the cascaded rectifier are tested.

Comparing Figs. 10(a) and 10(b), it can be seen that when the carrier inter-leaving phase shift control strategy is adopted, the voltage to earth of the H-bridge unit obviously fluctuates in a smaller magnitude than that having not adopt the strategy.

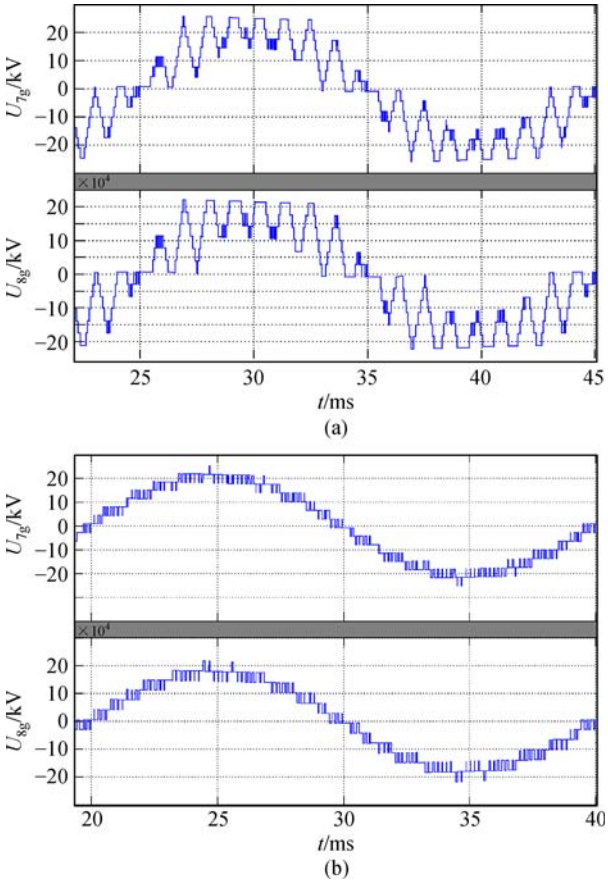

Fig. 10 Voltage of the H-bridge unit adopting (a) the carrier phase shift control strategy and (b) the carrier inter-leaving phase shift control strategy

5.2 Experimental verification of the grid-side control strategy

To verify effectiveness of the SSTT grid-side control strategy, a prototype of 4-level cascade with the capacity of 600 kV·A is set up for experiment. The DC side of the cascaded rectifier is connected to the LLC resonant converter, with the output of which connected to resistance. Parameters of the machine are shown in Table 2.

Table 2 Parameters of the experimental prototype

Parameters	Value
Grid voltage, U_s /kV	3.5–7.0
Rated power/(kV·A)	600
DC voltage, U_{dref} /V	3600
Cells of cascaded, N	2–4
HV-CHB cell switch frequency/Hz	450
Input Choke, L_s /mH	20
IGBT voltage grade of HV-parts/V	6500
IGBT voltage grade of LV-parts/V	3300
Ratio of transformer, M	2
Magnetic inductance, L_m /mH	10
Leakage inductance, L_r /μH	500–700
Resonance capacitance, C_r /μF	7–14
Output voltage, U_o /V	1800
Intermediate capacitance, C_{in} /μF	2000
Output capacitance, C_o /μF	1000–4000

5.2.1 Four-quadrant rectification of cascaded rectifier

A dual prototype is set up to verify the four-quadrant rectification and voltage balance control strategies. Tests are performed based on the four-quadrant control strategy for the synchronous rotating reference frame and interference resistance and response speed of the improved voltage outer loop. Modulation is conducted by adopting the single polarity double frequency carrier phase shift strategy. Figure 11 shows the waveforms of voltage and current in step response of the system under a rated load input. As the waveforms show, during rated-load input and cut-off, the drop amplitude of DC voltage does not exceed 200 V, and the response time of the grid-side current is less than 20 ms (1 linefrequency cycle). As shown in Fig. 12, when grid voltage drops by 10%, there is barely any fluctuation of DC voltage and grid-side current; when grid voltage drops by 20%, the fluctuations of DC voltage and grid-side current are separately less than 200 V and 40%, with the disturbance restoration time being 20 ms. Thus, the control strategy is proved to be of good resistance with a short response time.

5.2.2 Functional verification of harmonic suppression technology

The harmonic suppression control strategy is applied to the controller. As the cascaded rectifier mainly produces low-order harmonics (3rd, 5th, 7th, …) and due to the limitation of equivalent frequency of the rectifier, there are only 3 harmonic filtering channels (3rd, 5th, 7th) being set up in the controller when performing test on the 4-level cascaded rectifier. The Tectronix 3024B oscilloscope is used to collect waveforms of the output current i_c of the cascaded

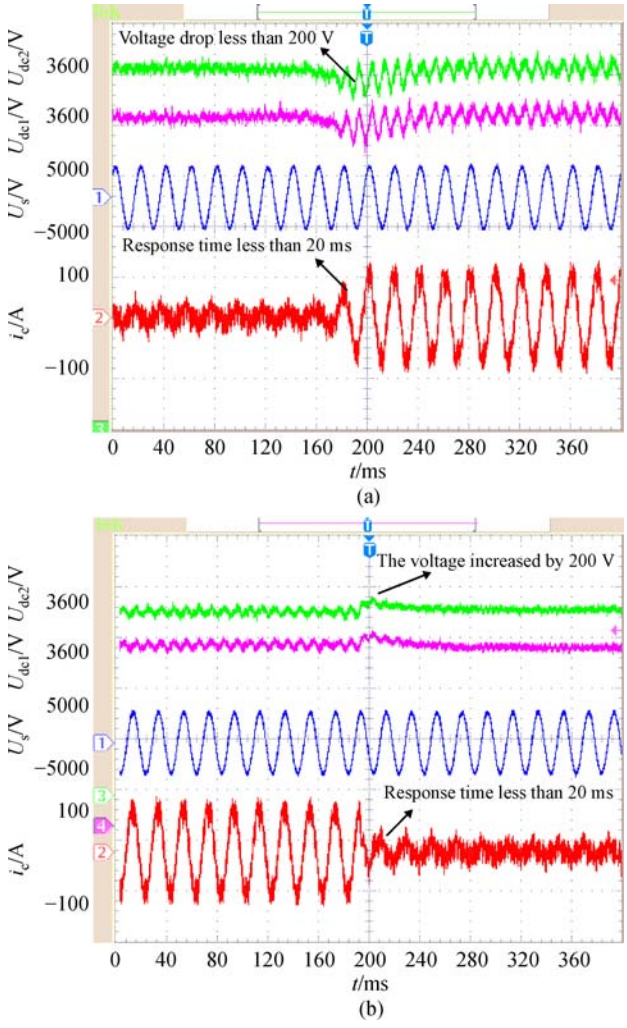

Fig. 11 Waveform of rated-load (a) input response and (b) cut-off response of the cascaded rectifier

rectifier. Fast Fourier transformation (FFT)analysis is conducted to compare the magnitude of the low-order harmonic components before and after application of the harmonic control strategy. As shown in Fig. 13(a), there is obvious current distortion before application of the harmonic control strategy. According to FFT analysis, amplitudes of the 3rd-, the 5th-, and the 7th-order harmonics are separately 4, 9 and 3 A. As shown in Fig. 13(b), after applying the harmonic control strategy, the content of current harmonic in the 3rd-, the 5th-, and the 7th-order harmonics paths are significantly reduced, with amplitudes approximating to 0 A. Figure 13(c) shows the steady-operation waveforms after the harmonic suppression strategy is implanted into the 4-level cascaded rectifier.

5.3 Experimental verification of beat frequency suppression

The LLC resonant converter is tested according to the parameters given in Table 2. As shown in Fig. 14, both the

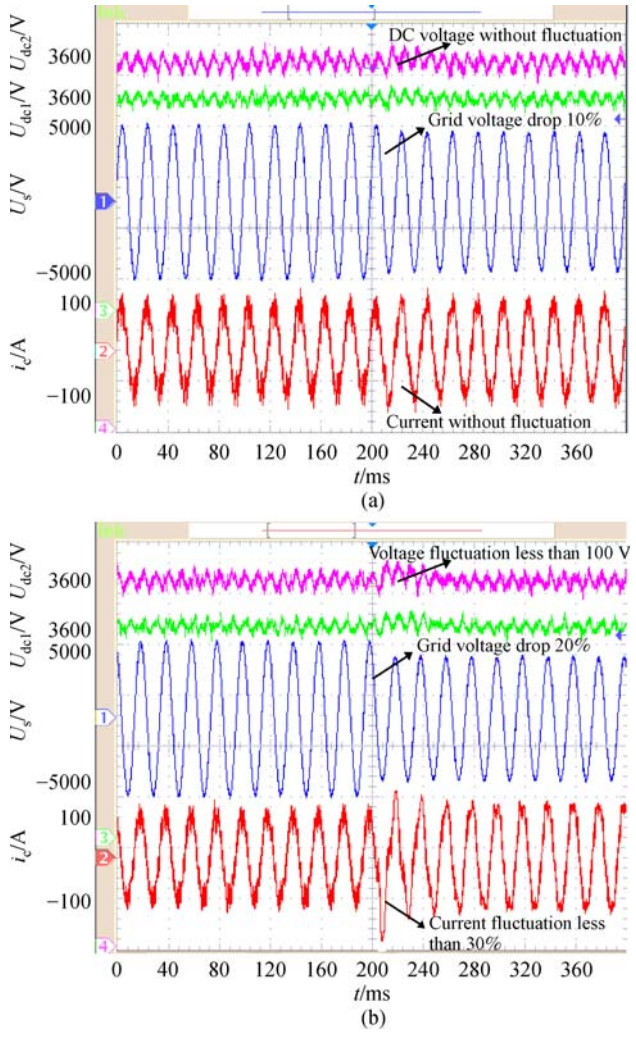

Fig. 12 Response waveform when grid voltage fluctuates by (a) 10% and (b) 20%

input and output voltages contain some secondary pulsating voltage. The primary-side resonant current i_r shows a secondary pulsating-shaped fluctuation. When current fluctuates to a higher value, the time of after flow will be shortened based on the same turn-off current, possibly resulting in the time of after flow of the diode being shorter than the dead zone time of the IGBT element. In such case, oscillation occurs in the output square-wave voltage, and end voltage of IGBT begins to recover from zero to the maximum value, when ZVS can not be realized and a significantly greater switch loss happens.

When the input/output capacitance C_o is changed to 700 μF and under the same power condition, current waveforms show the characteristics as shown in Fig. 15.

As shown in Fig. 15, under the same power condition, the input secondary pulsating voltage barely changes. When the output capacitance C_o is reduced, fluctuation of resonant current reduces significantly. However, although

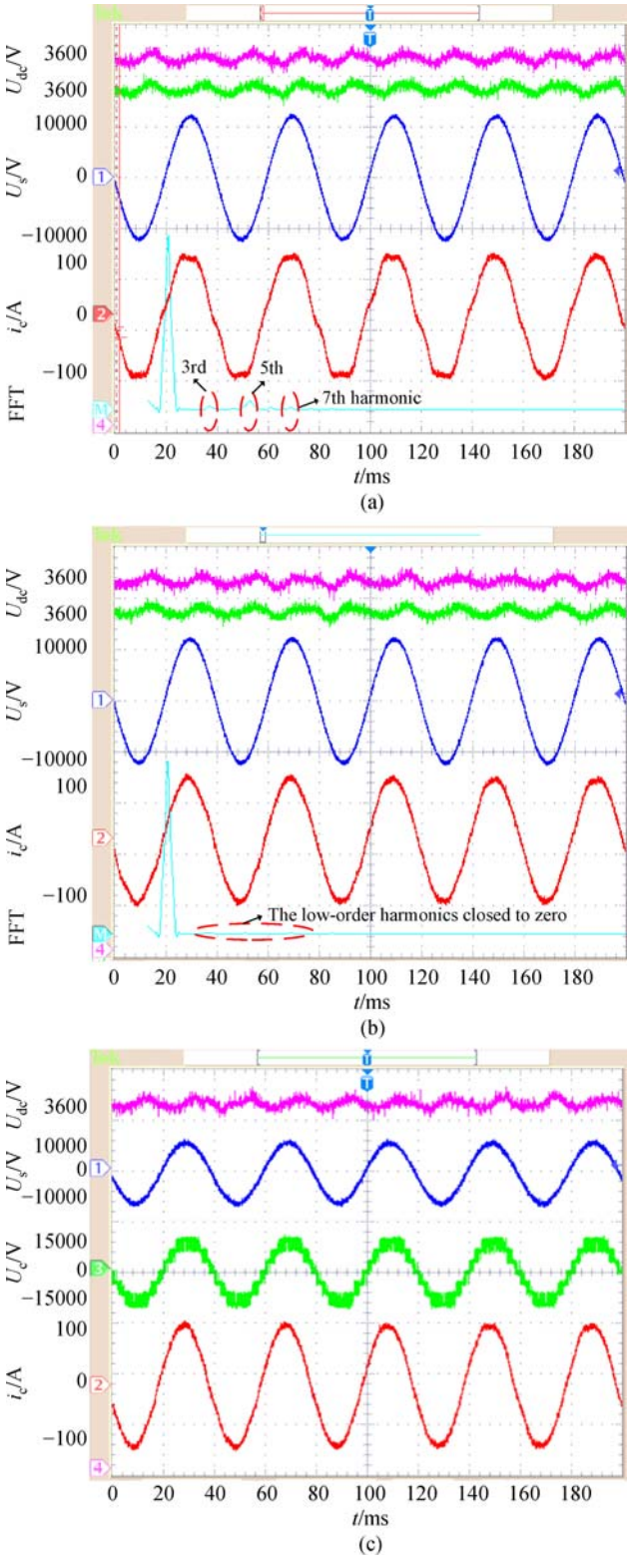

Fig. 13 (a) Current waveforms without the harmonic suppression strategy; (b) current waveforms with the 3rd-, the 5th-, and the 7th-order harmonics being filtered; (c) steady-operation waveforms with the harmonic suppression strategy

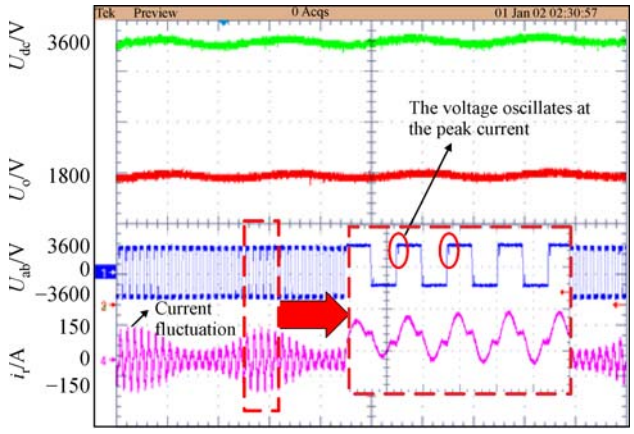

Fig. 14 Beat frequency of the LLC resonant converter

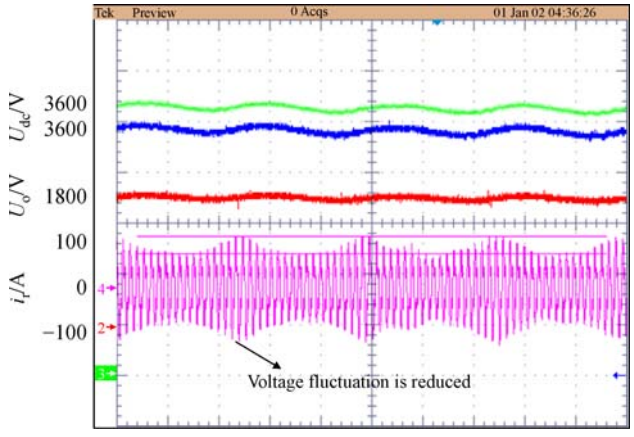

Fig. 15 Reduced current fluctuation of the LLC resonant converter

the reduction in the output capacitance C_o can suppress some current fluctuations caused by beat frequency, it cannot completely suppress current fluctuation. Reduced output capacitance leads to degraded dynamic performance of the output voltage. Therefore, it is necessary to improve control strategies (as mentioned before in Section 3.1) and increase LLC switch frequency so as to enhance dynamic performance of the output voltage.

5.4 Full-scale prototype experiment

To verify the SSTT, a full-scale prototype of 25 kV/1800 kV·A has been developed. Parameters of the prototype are listed in Table 3.

The developed high voltage SSTT prototype is modular and consists of several main assemblies as shown in Figs. 16 and 17. On the high AC-side, these include a main breaker, an input choke, and a start-up circuit that are connected to a number of identical cells in cascade. The start-up circuit is used to bring the energy from the grid to the DC link of the HV-CHBs during the start-up stage and is bypassed in the normal operation. Considering SSTT is

Table 3 Parameters of the full-scale prototype

Parameters	Value
Grid voltage, U_s /kV	25
Rated power/(kV·A)	1800
Max grid voltage/kV	31
Min grid voltage/kV	17.5
Rated frequency/Hz	50
DC voltage, U_{dref} /V	3600
Cells of cascaded, N	13
Cells of redundancy	1
HV-CHB cell switch frequency/Hz	450
Input choke, L_s /mH	20
IGBT voltage grade of HV-parts/V	6500
IGBT voltage grade of LV-parts/V	3300
Ratio of transformer, M	2
Magnetic inductance, L_m /mH	12.5
Leakage inductance, L_r /μH	700
Resonance capacitance, C_r /μF	7
Output voltage, U_o /V	1800
LLC switch frequency, f_s /Hz	1800–2200

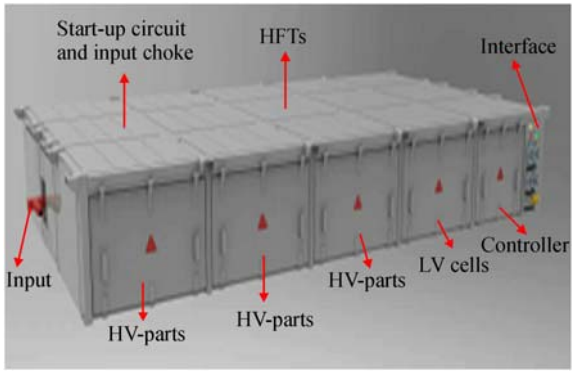

Fig. 16 SSTT prototype for 25 kV 50 Hz railway grid

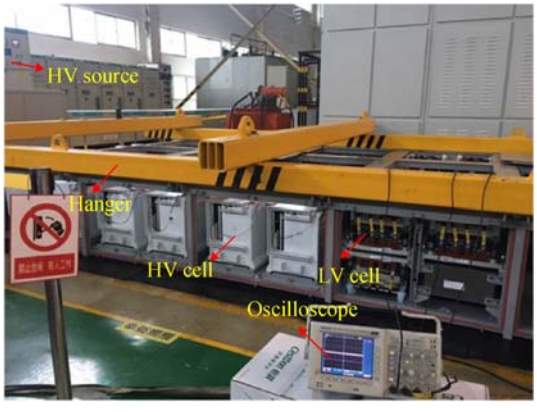

Fig. 17 The SSTT prototype is being tested

actually a converter connected directly to the HV AC grid, there is a need for some connected inductance at its input.

To meet the line voltage of a 25 kV 50 Hz railway grid and use the 6.5 kV IGBT modules with the purpose of keeping the number of switching devices at minimum. Twelve cells are used for series connection. To increase the availability of the SSTT, one redundancy cell is added which is used during normal operation. When failure in any of the cells, the error cell will be bypassed.

The HV side operates with 3600 V rated DC-link voltage. The LV side operates with 1800 V rated DC-link voltage, which provides DC source for the traction inverters. The DC-DC converter is of the LLC resonant type driven by the full-bridge configuration. Galvanic isolation is provided by the HFT, whose leakage and magnetizing inductances in combination with a resonant capacitor complete the resonant circuit.

The HFTs play three key roles. At first, they provide galvanic isolation between the HV side and the LV traction inverter. Secondary, they provide suitable voltage adaptation between HV DC-link and LV DC output. The third key function, they enable the HV IGBT modules to work in the ZVS mode and the LV IGBT modules to work in the ZCS mode, which will increase the overall efficiency of the system.

For the purpose of testing the availability of the 25 kV SSTT prototype in this paper, various functional experiments have been performed on the 18 kV grid voltage.

Figure 18 shows the characteristic obtained during with different loads connected to the output. Figure 18(a) shows the waveforms from the HV-CHB circuit. The CHB converter multilevel voltage is in phase with the grid voltage. The CHB converter current is closed to zero.

Figure 18(b) shows the waveforms from the HV-CHB circuit and LLC resonant converter. The Second harmonic ac ripple (100 Hz) is clearly visible in the output voltage. The voltage of the last HV cell (the nearest cell to the ground, U_{13}) is shown in CH2.The beat frequency

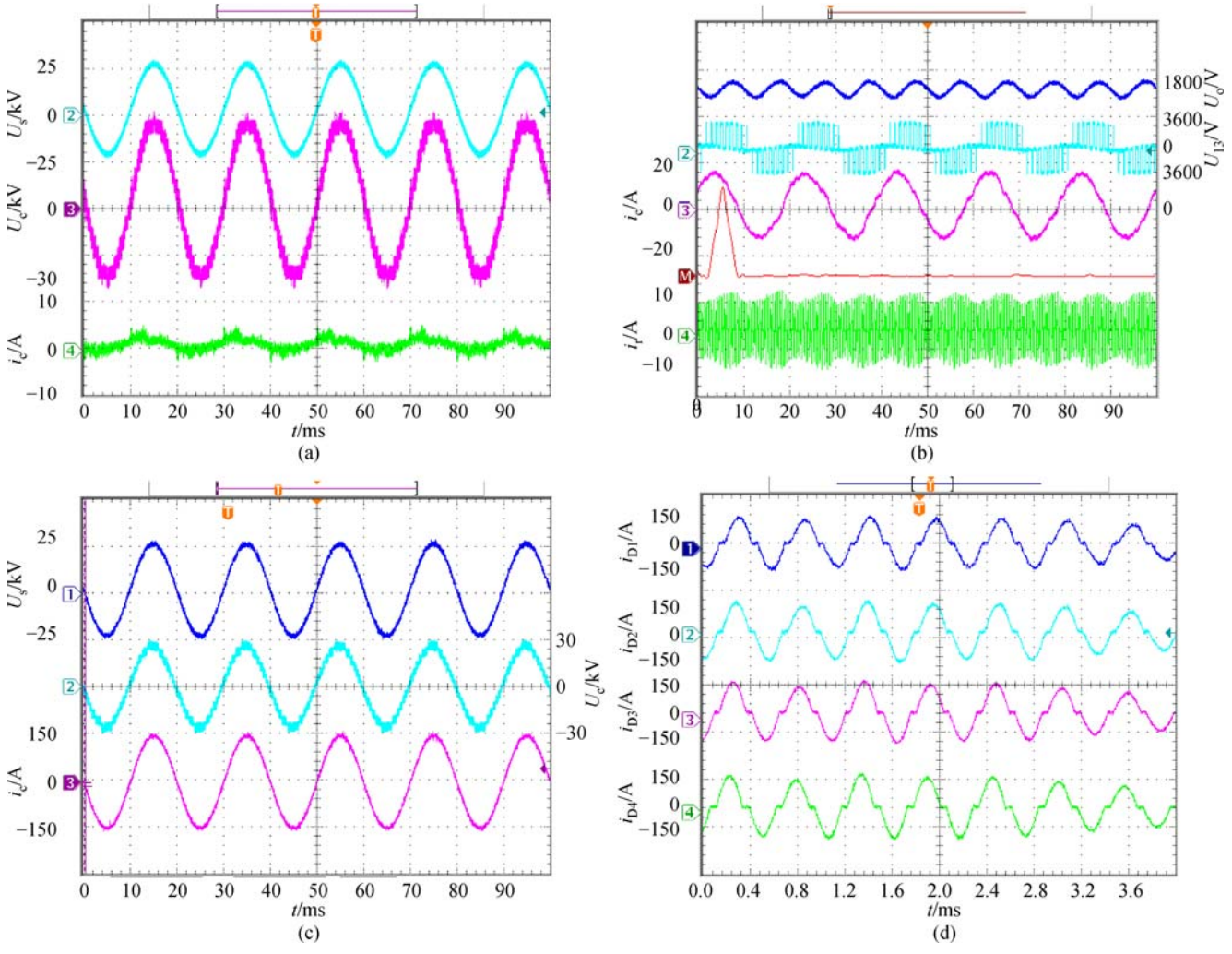

Fig. 18 Measured key waveforms of the 25 kV SSTT prototype with different loads: (a) Less than 50 kV·A; (b) 200 kV·A; (c) and (d) rated power 1800 kW

phenomenon still exists seen from CH4. Because as long as the second harmonic ac ripple exists, beat frequency phenomenon could be eliminated, but only be eased.

Figure 18(c) is shown the waveforms from the HV-CHB circuit at rated power. The CHB converter current is free of low-order harmonics and is in phase with the grid voltage, giving almost unity power factor. The resonant currents on the HFT secondary side as seen from Fig. 18(d) is almost identical.

6 Conclusions

The article introduces an SSTT-based traction drive system and compares it with conventional traction systems. Meanwhile, it also proposes a control strategy for the grid-side cascaded rectifier under the synchronous rotating reference frame and the carrier inter-leaving phase shift control strategy, and carries out optimized design for the LLC resonant converter. Specifically, conclusions are drawn as follows:

1) The new traction system uses SSTT to replace the original power traction transformer and four-quadrant rectifier, essentially, converting power frequency electricity into high-frequency electricity to improve power density of equipment and realize a smaller and lighter system.

2) The new traction system adopts the grid-side control strategy based on the synchronous rotating reference frame, with the grid-side response time shorter than 20ms and total harmonic distortion (THD) less than 1%. The voltage THD decreases along with increased number of cascades of the cascaded rectifier. When the number of cascades reaches a certain limit, the output voltage will be extremely close to sinusoid.

3) By parameters optimization, the DC-DC converter can mitigate the effect of beat frequency of inputted secondary pulsating voltage on the converter. Theoretically, secondary pulsating can be eliminated from outputted DC voltage by way of controlling the gain of the DC-DC converter. Certainly, the application of the secondary pulsation suppression strategy will inevitably increase current stress of power elements. In actual engineering design, details shall be further taken account of based on specific need.

4) With continuous innovation of and breakthroughs made in wide band gap (WBG) semiconductor device application, SiC elements can have a maximum voltage grade of 15 kV [31,32]. After commercialization of SiC elements featured in high voltage grade, high power level and high switch frequency, SSTT will be realized with obviously smaller volume and lighter weight, and efficiency of traction system will be further improved.

For the moment, the 25 kV and 1.8 MV·A full-power SSTT prototype still in testing by CRRC Zhuzhou Institute CO., LTD. is expected to realize a system efficiency over 96.5% depending on test results, with both volume and weight reducing by at least 20% from the original traction system. On-board examination will be carried out after testing on the traction system is completed. A major breakthrough in the domestic track traffic area can be anticipated with the application of the new generation of traction system.

References

1. Fu Y. The research of non-power frequency traction transformer conversion system based LLC resonant conversion. Thesis for the Master's Degree. Chengdu: Southwest Jiaotong Uninversity, 2015
2. Kouro S, Malinowski M, Gopakumar K, et al. Recent advances and industrial applications of multilevel converters. IEEE Transactions on Industrial Electronics, 2010, 57(8): 2553–2580
3. Allebrod S, Hamerski R, Marquardt R. New transformerless, scalable modular multilevel converters for HVDC-transmission. In: Proceedings of IEEE Power Electronics Specialists Conference. Rhodes: IEEE, 2008, 174–179
4. Song Q, Liu W, Li X, et al. A steady-state analysis method for a modular multilevel converter. IEEE Transactions on Power Electronics, 2013, 28(8): 3702–3713
5. Glinka M, Marquardt R. A new AC/AC multilevel converter family. IEEE Transactions on Industrial Electronics, 2005, 52(3): 662–669
6. Inoue S, Akagi H. A bidirectional isolated DC&DC converter as a core circuit of the next-generation medium-voltage power conversion system. IEEE Transactions on Power Electronics, 2007, 22(2): 535–542
7. Krismer F, Kolar J W. Accurate power loss model derivation of a high-current dual active bridge converter for an automotive application. IEEE Transactions on Industrial Electronics, 2010, 57(3): 881–891
8. Nymand M, Andersen M A E. High-efficiency isolated boost DC-DC converter for high-power low-voltage fuel-cell applications. IEEE Transactions on Industrial Electronics, 2010, 57(2): 505–514
9. Weigel J, Ag A N S, Hoffmann H. High voltage IGBTs in medium frequency traction power supply. In: Proceedings of 13th European Conference on Power Electronics and Applications. Barcelona: IEEE, 2009
10. Feng J, Chu W Q, Zhang Z, et al. Power electronic transformer based railway traction systems: Challenges and opportunities. IEEE Journal of Emerging and Selected Topics in Power Electronics, 2017, PP(99): 1
11. Zhao C, Dujic D, Mester A, et al. Power electronic traction transformer—Medium voltage prototype. IEEE Transactions on Industrial Electronics, 2014, 61(7): 3257–3268
12. Zhao C, Weiss M, Mester A, et al. Power electronic transformer (PET) converter: Design of a 1.2 MW demonstrator for traction applications. In: Proceedings of 2012 International Symposium on Power Electronics, Electrical Drives, Automation and Motion (SPEEDAM). Sorrento: IEEE, 2012, 855–860
13. Dujic D, Mester A, Chaudhuri T, et al. Laboratory scale prototype of a power electronic transformer for traction applications. In:

Proceedings of the 2011-14th European Conference on Power Electronics and Applications (EPE 2011). Birmingham: IEEE, 2011, 1–10

14. Dujic D, Steinke G K, Bellini M, et al. Characterization of 6.5 kV IGBTs for high-powermedium-frequency soft-switched applications. IEEE Transactions on Power Electronics, 2014, 29(2): 906–919
15. Besselmann T, Mester A, Dujic D. Power electronic traction transformer efficiency improvements under light-load conditions. IEEE Transactions on Power Electronics, 2014, 29(8): 3971–3981
16. Falcones S, Mao X, Ayyanar R. Topology comparison for solid state transformer implementation. In: Proceedings of 2010 IEEE Power and Energy Society General Meeting. Minneapolis: IEEE, 2010, 1–8
17. Shi J, Gou W, Yuan H, et al. Research on voltage and power balance control for cascaded modular solid-state transformer. IEEE Transactions on Power Electronics, 2011, 26(4): 1154–1166
18. Zhao T, Wang G, Bhattacharya S, et al. Voltage and power balance control for a cascaded H-bridge converter-based solid-state transformer. IEEE Transactions on Power Electronics, 2013, 28(4): 1523–1532
19. Huber J E, Kolar J W. Common-mode currents in multi-cell solid-state transformers. In: Proceedings of 2014 International Power Electronics Conference. Hiroshima: IEEE, 2014, 766–773
20. Marchesoni M, Novaro R, Savio S. AC locomotive conversion systems without heavy transformers: Is it a practicable solution? In: Proceedings of the 2002 IEEE International Symposium on Industrial Electronics. IEEE, 2002, 4: 1172–1177
21. Dujic D, Kieferndorf F, Canales F. Power electronic transformer technology for traction applications—An overview. Electronics, 2012, 16(1): 50–56
22. Oliveira D S, de A Honorio D, Barreto L H S C, et al. A two-stage AC/DC SST based on modular multilevel converter feasible to AC railway systems. In: Proceedings of 2014 Twenty-Ninth Annual IEEE Applied Power Electronics Conference and Exposition (APEC). Fort Worth: IEEE, 2014, 1894–1901
23. Feng X. AC Electrical Drives & Control System. Beijing: Higher Education Press, 2009, 272–273 (in Chinese)
24. Zhou M, You X, Wang C, et al. Switching angle calculation and harmonic analysis of current harmonic minimum PWM. Proceedings of the CSEE, 2014, 34(15): 2362–2370 (in Chinese)
25. Gou B, Feng X, Song W, et al. Analysis and suppression of beat phenomenon for railway traction converters and motors. Proceedings of the CSEE, 2013, 33(9): 55–63 (in Chinese)
26. Liu H, Jiao Y, Ming D. Unified power quality controller based on synchronous rotating coordinates. High Power Converter Technology, 2015, 4: 39–43
27. Jiang Y, Cao Y, Gong Y. Research on the cascade multilevel inverter based on different carrier phase-shifted angle. Proceedings of the CSEE, 2007, 27(1): 76–81 (in Chinese)
28. Holmes D G, McGrath B P. Opportunities for harmonic cancellation with carrier-based PWM for two-level and multilevel cascaded inverters. IEEE Transactions on Industry Applications, 2001, 37: 564–582
29. Salam Z, Goodman C. Compensation of fluctuating DC link voltage for traction inverter drive. In: Proceedings of IEEE Sixth International Conference on Power Electronics and Variable Speed Drives. Nottingham: IEEE, 1996: 390–395
30. Wang J, Lu X, Zhang F, et al. Low frequency input current ripple analysis and reduction in a single phase inverter with two-stage structure. Proceedings of the CSEE, 2012, 32(6): 10–16 (in Chinese)
31. Kadavelugu A, Bhattacharya S. Design considerations and development of gate driver for 15 kV SiC IGBT. In: Proceedings of 2014 Twenty-Ninth Annual IEEE Applied Power Electronics Conference and Exposition (APEC). Fort Worth: IEEE, 2014, 1497–1501
32. Kadavelugu A, Bhattacharya S, Ryu S H, et al. Understanding dv/dt of 15 kV SiC N-IGBT and its control using active gate driver. In: Proceedings of 2014 IEEE Energy Conversion Congress and Exposition (ECCE). Pittsburgh: IEEE, 2014, 2213–2220